Pumping Fluids with Periodically Beating Grafted Elastic Filaments

Yong Woon Kim[1,2] and Roland R. Netz[1]

[1]*Physics Department, Technical University Munich, 85748 Garching, Germany*
[2]*Department of Physics and Materials Research Laboratory, University of California at Santa Barbara,
Santa Barbara, California 93106, USA*
(Received 19 October 2005; published 21 April 2006)

Using Brownian dynamics simulations, we investigate the pumping efficiency of an array of periodically beating semiflexible filaments that are grafted to a surface. Full hydrodynamic interactions among and within filaments and no slip at the surface are considered. Optimal pumping is obtained for a characteristic ratio of applied forward-backward torques and filament persistence length. For independently driven filaments, phase locking between neighboring filaments occurs autonomously via hydrodynamic coupling, giving rise to significantly enhanced pumping efficiency.

Cilia and flagella are essential building blocks for locomotion of microorganisms and fluid transport in digestive and respiratory organs. Their design principles are the evolutionary answer to the need for generating thrust on the micron spatial and velocity scales of cellular biology [1]. Since the seminal work by Taylor where the synchronization of two waving sheets was discussed [2], flagellar motion and beating dynamics have attracted considerable attention [3,4]. Self-propulsion in a viscous fluid using surface distortions or chemical reactions has also been proposed [5]. Because of the linearity of the Stokes equation, no net thrust is generated by time-reversal reciprocal motions. Actually, cilia *in vivo* show distinct spatiotemporal beating patterns in the forward and backward strokes, which leads to directed propulsion [6]. Of particular interest to theorists has been metachronal coordination where adjacent cilia beat in a constant phase lag, giving wavelike patterns [7,8]. The microscopic mechanism behind the symmetry breaking between back-and-forth strokes remains largely obscure, and therefore most previous studies treated the biologically observed ciliary motions as an input parameter [7,8]. It is therefore not easy to generalize this scheme to the synthetic world and use it, e.g., for the controlled pumping of fluids with grafted elastic filaments in nano-chip-sized devices.

Recent technical developments have enabled the manufacture of synthetic molecular motors for regulated motion on the nanoscale: molecular devices transforming chemical [9] or optical [10,11] energy into rotary motion have been reported. Likewise, beating filaments could be realized with the help of optically active chemical groups such as azo-benzene, which convert optical energy into mechanical (pulling or pushing) force [12]: by optical excitations, the azo-benzene group shows a periodic configurational change, and can thus lead to a cyclic beating of a filament when used as a hinge linking the filament to the surface. Furthermore, a condensed monolayer of molecular motors undergoing coherent motion has been successfully fabricated [13].

Motivated by this, we study the pumping or propulsion efficiency of a system consisting of periodically beating elastic filaments anchored to a solid surface, possibly useful for pumping and stirring in nanofluidic devices. As appropriate for a minimal synthetic design, external torques are applied at the grafting sites in a temporal asymmetric pattern leading to a slow and fast stroke. The competition between hydrodynamic friction and rod elasticity breaks the spatial symmetry, showing cilialike beating shapes and giving rise to a net pumping. Interestingly, and in contrast to the biological cilia system [8], it is the slow stroke that determines the pumping direction. A scaling law for the various elastic parameters of the pumping device is derived at which optimal performance is achieved and compared with numerical results. For a certain range of filament elasticity, self-organized synchronization between neighboring filaments develops, with considerable consequences on the pumping efficiency.

We employ Brownian dynamics simulations with full hydrodynamic interactions among filaments, and treat the surface as a no-slip boundary for the ambient fluid. The filament is modeled as a chain of N connected spherical beads with radius a; following the extensible wormlike chain model, the elastic potential energy reads as $U = \sum_{i=1}^{N-1}[(\gamma/4a)(r_{ii+1} - 2a)^2 + (\epsilon/2a)(1 - \cos\theta_i)]$, where $r_{ij} = |\mathbf{r}_i - \mathbf{r}_j|$ and θ_i is the angle between neighboring bonds $\mathbf{r}_{i-1i}$ and $\mathbf{r}_{ii+1}$. The parameters γ and ϵ are the stretching and bending moduli, respectively; for an isotropic elastic rod, $\epsilon/\gamma = a^2/4$. The persistence length follows as $l_p = \epsilon/k_BT$ and the length of an unstretched filament is $l = 2aN$. At low Reynolds number (i.e., in the inertialess regime), the dynamics of the ith bead is given by the position Langevin equation [14],

$$\dot{\mathbf{r}}_i(t) = -\sum_j \boldsymbol{\mu}_{ij}(\mathbf{r}_i, \mathbf{r}_j)\nabla_{\mathbf{r}_j}U + \boldsymbol{\mu}_{i2}\frac{\mathbf{r}_{12} \times \boldsymbol{\tau}(t)}{r_{12}^2} + \boldsymbol{\xi}_i. \quad (1)$$

Hydrodynamic interactions are incorporated via a multipole expansion of the mobility tensor $\boldsymbol{\mu}_{ij}$ in terms of the

bead radius a as [14]

$$\mu_{ij}^{\alpha\beta}(\mathbf{r}_i, \mathbf{r}_j) = \left(1 + \frac{a^2}{6}\nabla_{\mathbf{r}_i}^2\right)\left(1 + \frac{a^2}{6}\nabla_{\mathbf{r}_j}^2\right)G_{\alpha\beta}(\mathbf{r}_i, \mathbf{r}_j), \quad (2)$$

where $G_{\alpha\beta}$ is the hydrodynamic Green's function in the presence of a no-slip wall at $z = 0$ (the self mobility is constant, $\mu_{ii}^{\alpha\beta} = \mu_0\delta_{\alpha\beta}$) [7]. As synthetic motors are typically smaller than natural cilia, random thermal motion becomes significant and is thus included. The vectorial random forces acting on two particles are correlated according to $\langle\boldsymbol{\xi}_i^\alpha(t)\boldsymbol{\xi}_j^\beta(t')\rangle = 2k_BT\mu_{ij}^{\alpha\beta}(\mathbf{r}_i, \mathbf{r}_j)\delta(t - t')$. We model the effect of a motor at the base by applying a temporal torque profile $\tau(t)$ on the second monomer (with the first monomer fixed on the surface), consisting of two phases: in the slow stroke, a relatively small torque τ_s is applied to swing the filament in the clockwise direction as in the left part of Fig. 1(a). When the angle between the first bond $\mathbf{r}_{12}$ and the planar surface reaches a threshold angle ϕ_{max}, a strong torque $-\tau_f$ is exerted in the reverse direction [right part of Fig. 1(a)], which initiates the fast stroke. When the threshold angle is reached again, the beating pattern is repeated from the beginning. For numerical iterations, we discretize the Langevin equation with a

FIG. 1 (color online). (a) Snapshots of the elastic filament driven by the slow (left) and fast (right) stroke: $N = 20$, $l_p/l = 2 \times 10^5$, $\tau_s = 2 \times 10^5 k_BT$, $\phi_{max} = \pi/6$, $\rho = 0.0005$, and torque ratio $\alpha = 4$. Here n refers to the number of simulation steps. Note that the number of steps between successive snapshots is 5 times larger in the slow stroke. (b) Lateral flow profile as a function of distance from the no slip wall. The number indices refer to corresponding conformations in (a). (c) Temporal evolution of bulk solvent velocity $\tilde{v}_\infty$ over a few beating cycles. (d) Snapshots of a stiffer filament for the same parameters as in (a) but persistence length $l_p/l = 10^6$.

time step Δ, rescale all lengths by the monomer radius a according to $\tilde{\mathbf{r}} = \mathbf{r}/a$, and rescale all energies by the torque in the slow stroke, according to $\tilde{U} = U/\tau_s$. Therefore we get the rescaled bare mobility $\tilde{\mu}_0 = \Delta\tau_s\mu_0/a^2$, which is chosen as $\tilde{\mu}_0 = 0.001$. In the first part we simulate a single filament explicitly inside a square unit cell with linear size L and treat hydrodynamic interactions via two-dimensional periodic boundary condition imposed on the flow field. This situation corresponds to an array of filaments that are synchronized externally. The grafting density is defined as $\rho = a^2/L^2$.

Shown in Fig. 1(a) are representative chain snapshots under weak (left) and strong (right) applied torques. The ratio of external torques, $\alpha = |\tau_f|/|\tau_s|$, is set to $\alpha = 4$ in Fig. 1. While the filament remains almost straight during the slow stroke, it is significantly bent in the fast stroke, caused by increased frictional forces. The typical conformation depends on the ratio of chain stiffness (l_p/l) and applied torque (τ_s/k_BT), as is realized from the snapshots in Fig. 1(d) where the persistence length is increased by a factor of 5 as compared to Fig. 1(a). Figure 1(b) shows the laterally averaged and rescaled flow profile along the beating direction (x direction), $\tilde{v}(z) = \Delta v(z)/a$, at different times as a function of distance from the surface. It follows from the laterally averaged Green's function

$$\bar{G}(z, z') = \int dxdy\, G_{xx}(x, y, z, z') = \frac{z + z' - |z - z'|}{2\eta} \quad (3)$$

by summing over the forces $\mathbf{f}_i = \nabla_{\mathbf{r}_i}U + \delta_{i2}\mathbf{r}_{12} \times \boldsymbol{\tau}(t)/r_{12}^2$ acting on a monomer at height z_i as $v(z) = \sum_i \bar{G}(z, z_i)f_i^x\rho/a^2$. Depicted in Fig. 1(c) is the bulk fluid velocity (determined at a distance $\tilde{z} = 40$ beyond which it is constant), $\tilde{v}_\infty = \Delta v_\infty/a$, in the course of repeated beating cycles. In compliance with the externally applied torque, $\tilde{v}_\infty$ changes sign. By integrating $\tilde{v}_\infty$ with respect to one period T, we can calculate the net displacement over which the ambient fluid is transported during one cycle, $D = \int_T dt v_\infty(t)$, which is a measure of the directed pumping of our synthetic cilia. Because of the asymmetry in the velocity time evolution, the net pumping velocity is nonzero. In order to estimate the pumping (or propulsion) efficiency, we divide the pumping distance D by the total energy input per one cycle, $E = (\pi - 2\phi_{max})(\tau_s + \tau_f)$. We arrive at the unitless efficiency $\eta = (D/a)/(E/k_BT)$.

Figure 2(a) displays the efficiency η as a function of persistence length for three different torques τ_s at a fixed torque ratio of $\alpha = 3$: $\tau_s = 2 \times 10^3 k_BT$ (circles), $2 \times 10^4 k_BT$ (triangles), and $2 \times 10^5 k_BT$ (diamonds). Data are averaged over ten repeated beating cycles in a stationary state after a few transient cycles. The efficiency has a pronounced maximum for a certain persistence length, and this optimal persistence length increases with the applied torque strength. Thermal agitation makes the data quite noisy with decreasing τ_s (circles), while the curve is very smooth for elevated τ_s (diamonds).

The general mechanism behind net propulsion or pumping is similar to the biological cilia system: In the slow stroke the filament retains an upright conformation and the entraining effect on the surrounding liquid is maximized since (i) the filament is oriented perpendicular to the direction of motion (leading to a large hydrodynamic friction) and (ii) the distance to the no slip wall is largest. Equation (3) shows that the averaged lateral fluid velocity due to a force is indeed linearly proportional to the distance of the force locus from the no-slip wall. In the fast stroke, on the other hand, the filament is bent and thus not strictly perpendicular to the direction of motion and closer to the surface. In contrast to the biological cilia system, it is the slow stroke that is less bent and dominates the net pumping. For optimal performance (distinct viscous resistances in two phases), the filament conformations should thus be very different in the fast and slow strokes, namely, almost straight in the slow stroke and very bent in the fast stroke. In order to maintain a straight conformation in the slow stroke, the internal stress due to the applied torque has to be balanced by bending elasticity, yielding a simple scaling relationship, $\epsilon \sim \tau_s l$, or

$$l_p/l \approx \tau_s/k_B T. \qquad (4)$$

This scaling law is quantitatively confirmed by the numerical results in Fig. 2(b), where efficiency is plotted as a function of l_p/l and $\tau_s/k_B T$ (bright color corresponds to high efficiency and vice versa).
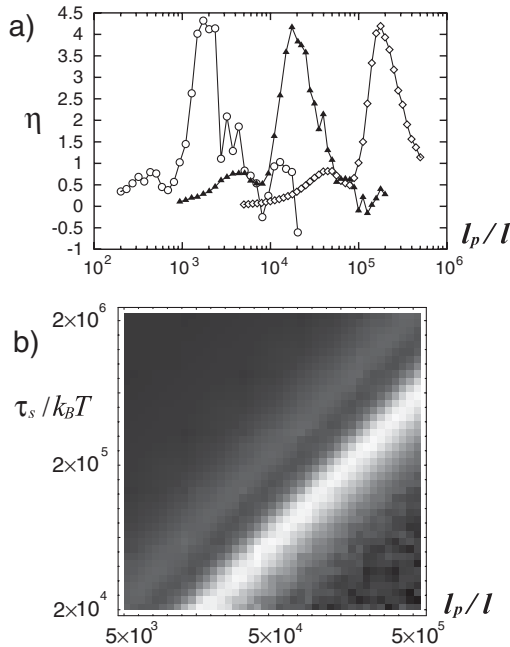
FIG. 2. (a) Efficiency η vs persistence length for different torque strengths: $\tau_s = 2 \times 10^3 k_B T$ (circles), $2 \times 10^4 k_B T$ (triangles), and $2 \times 10^5 k_B T$ (diamonds). (b) Contour plot of efficiency η as a function of l_p/l and $\tau_s/k_B T$. The brighter, the more efficient. The linear relationship between $\tau_s/k_B T$ and l_p/l for maximal efficiency is clearly seen. For all data, parameters are chosen as $\alpha = 3$, $\phi_{max} = \pi/4$, and $\rho = 0.001$.

The other important control parameter is the ratio of the applied forward-backward torques, $\alpha = \tau_f/\tau_s$. We display in Fig. 3 the efficiency as a function of filament stiffness l_p/l and α at a fixed τ_s. Most efficient thrust is obtained around $\alpha = 3$, at the same time the scaling relation Eq. (4) is obeyed. For $\tau_f \approx \tau_s$ the motion is reciprocal so that net pumping is impossible. On the other hand, a too fast stroke $\tau_f \gg \tau_s$ leads to a considerable stretching of the filament, not leaving the distal part enough time to catch up with the base motion.

It was suggested that for the biological cilia system metachronal coordination of multicilia configuration may occur via hydrodynamic coupling [6,8,15]. Up to now we have considered filaments that are synchronized externally, which is appropriate when filaments are moved by optical motors that would be collectively excited by laser pulses. On the other hand, motor designs that lead to independent beatings for individual filament are also conceivable, it is therefore intriguing to study autonomously driven but hydrodynamically coupled filaments within the present model: let us consider two identical elastic filaments, placed $L/2$ apart in open boundary condition, which are driven by identical but independent motors. We define the phase difference between the two filaments, $\Delta\phi = \phi_1 - \phi_2$, by the angle the base of the second filament makes with the surface (ϕ_2) when the first filament is at its turning point from fast to slow stroke ($\phi_1 = \pi - \phi_{max}$). Figure 4(a) exhibits the evolution of the phase difference for various initial conditions as a function of the number of beatings m. As is clearly seen, the filaments spontaneously synchronize after a few beating cycles and beat with a constant phase lag (phase locking), independent of the initial phase differences (more clearly seen in the inset). The final value of phase locking depends on the system parameters, as demonstrated in Fig. 4(b) (solid symbols) where $\Delta\phi$ is depicted with increasing l_p. This indicates that the dynamics is very cooperative and the existence of neighboring cilia is important, due to long-range hydrodynamic interaction in Stokes flow. Note also that a finite
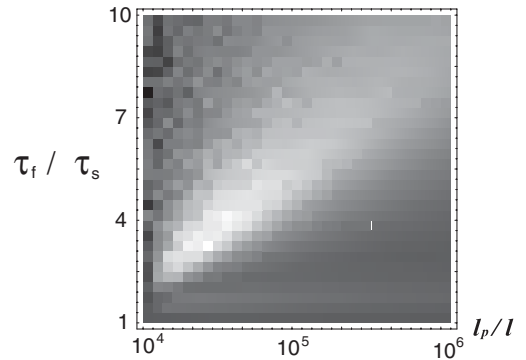
FIG. 3. Contour plot of efficiency as a function of $\alpha = \tau_f/\tau_s$ and l_p/l at fixed $\tau_s = 2 \times 10^4 k_B T$. The brighter, the more efficient. The optimal ratio of τ_f/τ_s is found to be around 3. The used parameters are $\rho = 0.001$ and $\phi_{max} = \pi/4$.
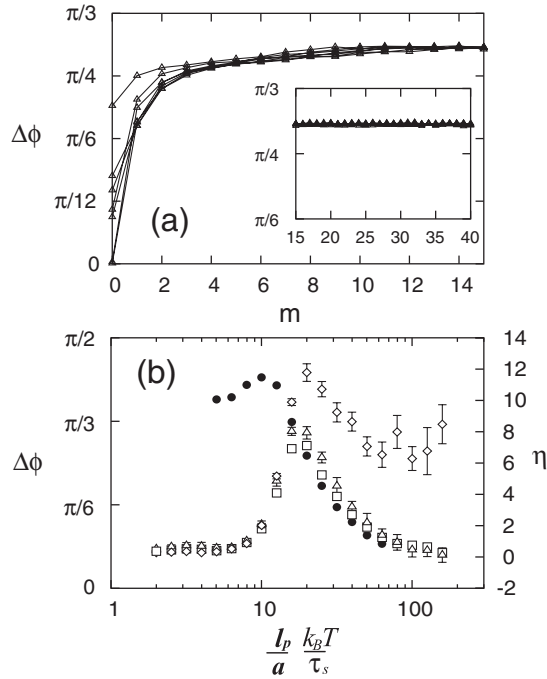
FIG. 4. (a) Phase difference between two cilia vs the number of beating cycles m for several initial phase differences. Inset indicates phase locking in the longtime limit. The parameters are $\tau_s = 2 \times 10^5 k_B T$, $\alpha = 3$, $\phi_{max} = \pi/4$, $l_p/l = 2 \times 10^5$, and $\rho = 0.001$. (b) Efficiency η vs l_p: for one cilium per unit cell with periodic boundary ($\Delta\phi = 0$, squares), for one cilium with open boundary (triangles), and for two cilia (diamonds) with variable $\Delta\phi$, which is denoted by solid circles. The parameters are the same as (a) except for $\rho = 0.002$.

flexibility is essential for the synchronization and no synchronization occurs when the filaments are too stiff [16].

Let us explore the consequences of phase locking on the pumping efficiency. For this purpose, we plot the efficiency η in the stationary synchronized state (after about 30 transient beating cycles) in Fig. 4(b) as a function of the rescaled stiffness $l_p k_B T/a\tau_s$ as suggested by Eq. (4). The case of a single filament (squares) corresponds to a periodic system with zero phase difference, the data for two filaments (open diamonds) are obtained at the same grafting density of chains and correspond to a variably synchronized state. For comparison, a single filament with open boundary is also simulated (triangles), implying that periodic boundary conditions are not so important as the laterally averaged solvent flow profiles are concerned (they play a somewhat larger role for filament velocities). Interestingly, the efficiency is significantly enhanced in the system allowing for variable synchronization, which means that the system prefers and finds a state of maximal pumping efficiency using hydrodynamic couplings in a self-organized fashion [2]. We stress that the relationship of Eq. (4) for optimal performance seems still valid, even

in the occurrence of phase locking (η is maximal at roughly the same l_p).

The pumping efficiency depends on other control parameters as well. For instance, in the case of two independently beating filaments, maximal pumping efficiency is obtained when the boundary angle for geometric switching is $\phi_{max} \approx \pi/4$, while in the single rod case the efficiency monotonically decreases with increasing ϕ_{max}. It is interesting to note that the cilia of *Paramecium* approximately sweep an angle of about $\pi/2$ during the power stroke. It is also found that the beating frequency rises as a result of cooperative dynamics unless the chains are very flexible. Predictions made in this work can be easily tested by recently proposed macroscopic scale models of centimeter-sized filaments that are driven by a stepper motor in a high-viscosity silicone oil, which were used to study bundling of flagella [17].

[1] E. M. Purcell, Am. J. Phys. **45**, 3 (1977).
[2] G. Taylor, Proc. R. Soc. A **209**, 447 (1951); **211**, 225 (1952).
[3] J. J. L. Higdon, J. Fluid Mech. **90**, 685 (1979).
[4] S. Camalet, F. Jülicher, and J. Prost, Phys. Rev. Lett. **82**, 1590 (1999).
[5] H. A. Stone and A. D. T. Samuel, Phys. Rev. Lett. **77**, 4102 (1996); R. Golestanian, T. B. Liverpool, and A. Ajdari, Phys. Rev. Lett. **94**, 220801 (2005).
[6] M. A. Sleigh, *Cilia and Flagella* (Academic, London, 1974).
[7] J. R. Blake, J. Fluid Mech. **55**, 1 (1972); N. Liron and S. Mochon, *ibid.* **75**, 593 (1976); M. C. Lagomarsino, P. Jona, and B. Bassetti, Phys. Rev. E **68**, 021908 (2003).
[8] S. Gueron and K. Levit-Gurevich, Proc. Natl. Acad. Sci. U.S.A. **96**, 12 240 (1999).
[9] T. R. Kelly, H. D. Silva, and R. A. Silva, Nature (London) **401**, 150 (1999).
[10] N. Koumura *et al.*, Nature (London) **401**, 152 (1999).
[11] T. Harada and K. Yoshikawa, Appl. Phys. Lett. **81**, 4850 (2002).
[12] T. Hugel, N. B. Holland, A. Cattani, L. Moroder, M. Seitz, and H. E. Gaub, Science **296**, 1103 (2002).
[13] Y. Tabe and H. Yokoyama, Nat. Mater. **2**, 806 (2003).
[14] D. L. Ermak and J. A. McCammon, J. Chem. Phys. **69**, 1352 (1978).
[15] L. Gheber and Z. Priel, Cell Motil. Cytoskeleton **39**, 9 (1998).
[16] M. Kim and T. R. Powers, Phys. Rev. E **69**, 061910 (2004); M. Reichert and H. Stark, Eur. Phys. J. E **17**, 493 (2005).
[17] M. Kim *et al.*, Proc. Natl. Acad. Sci. U.S.A. **100**, 15 481 (2003).